Efficiency Assessment for Crop Classification Using Multi-Sensor Data in Google Earth Engine

Farhad Ullah[1], Sawaid Abbas[1,2,*], Muhammad Usman[3], Aftab Ameen[1], Zulfiqar Ali Abbas[1], Syed Muhammad Irteza[4], Sami Ullah Khan[5]

[1]Smart Sensing for Climate and Development, Center for Geographical Information System, University of the Punjab, Lahore, Pakistan

[2]Department of Land Surveying and Geo-Informatics, The Hong Kong Polytechnic University, Hong Kong SAR

[3]Interdisciplinary Research Center for Aviation and Space Exploration, King Fahd University of Petroleum and Minerals, Dhahran, Saudi Arabia

[4]Punjab Information Technology Board, Lahore

[5]Urban Unit, Lahore

[*]**Correspondence:** sawaid.gis@pu.edu.pk (S.A); sawaid.abbas@connect.polyu.hk

Citation | Ullah. F, Abbas. S, Usman. M, Ameen. A, Abbas. Z. A, Irteza. M. S, Khan. S. U, "Efficiency Assessment for Crop Classification Using Multi-Sensor Data in Google Earth Engine", IJIST, Special Issue pp 294-304, June 2024

DOI | https://doi.org/10.33411/IJIST/862

Received | June 03, 2024; **Revised |** June 07, 2024; **Accepted |** June 13, 2024; **Published |** June 19, 2024.

Accurate mapping of agricultural lands and crop distribution is crucial for food security, sustainable development, and informed policymaking. This research classified agricultural crops in the Rahim Yar Khan district of Pakistan using multi-sensor images from Sentinel-1 and Sentinel-2 satellites. The study employed the cloud computing platform Google Earth Engine (GEE) and compared the performance of the Random Forest (RF) algorithm using Sentinel-1 (VV, HV, and HV+VV), Sentinel-2, and integrated datasets. Ground truth information obtained from field surveys and high-resolution images served as reference samples for training and validation. The fusion of Sentinel-1 and Sentinel-2 data enhanced feature extraction, leading to improved crop type classification. Post-processing procedures ensured that the maps were visually clear and free of noise, allowing for accurate crop mapping and land cover categorization. The classification results indicated high accuracy for crops such as sugarcane, cotton, rice, and water bodies. The RF classifier using fused data achieved the highest accuracy (overall accuracy of 93% and Kappa coefficient of 90%), followed by Sentinel-2 (89%), Sentinel-1 VV+VH (72%), Sentinel-1 VH (66%), and Sentinel-1 VV (62%). The study underscores the value of data integration in improving the classification accuracy of major crops (sugarcane, cotton, and rice) in the region. While some classes showed exceptional accuracy, others, such as Orchard, require further refinement in categorization methods. Overall, the study provides valuable insights into using multi-sensor remote sensing data for agricultural monitoring and decision-making.

Keywords: Machine learning, Crop classification, Sentinel-1, Sentinel-2, Google Earth Engine.

Introduction:

In 2020, the number of people facing hunger in the Asia and Pacific region reached 375.8 million [1]. This situation is further compounded by the fact that 1.1 billion individuals lacked access to adequate food, highlighting a serious issue of food security. Accurate and timely quantification of agricultural crops and their geographical distribution is crucial for ensuring food security [2]. Crop mapping is also essential for forecasting crop production and assessing agricultural statistics [3], which helps in evaluating food demands. Satellite remote sensing has enabled in-season crop classification using multispectral imagery [4][5][6].

In June 2015, the European Space Agency (ESA) launched the Sentinel-2 mission, which includes two identical satellites, Sentinel-2A and Sentinel-2B. These satellites provide high-resolution (10 m) imagery with a five-day revisit period due to their ten-day individual return cycle. The multispectral instrumentation (MSI) on Sentinel-2 offers data with 13 spectral bands in the visible, near-infrared, and shortwave infrared regions [7][8]. Despite the high temporal frequency of observations, optical data can be hindered by cloud cover, creating gaps in time series and reducing the accuracy of crop type identification [9][10][11].

To address this issue, microwave remote sensing can provide additional information for land cover and land use (LCLU) classification, as it penetrates through clouds without significant interference due to its longer wavelengths [12]. Synthetic Aperture Radar (SAR), a microwave-based imaging technology, has enhanced our understanding of earth resources [13]. Since the launch of the Sentinel-1 mission by ESA, SAR-based applications for crop classification have increased. While both Sentinel-1A and Sentinel-1B initially provided observations every six days, currently only Sentinel-1A is operational, offering repeat coverage every twelve days [12].

To develop dense time series and extract information from integrated datasets, this study utilized Google Earth Engine (GEE), a non-profit cloud computing platform for geographic spatial analysis [14]. GEE is widely used in large-scale remote sensing applications, including forest monitoring, crop yield estimation, and crop mapping [15]. The variety of datasets available in GEE provides a reliable source for accurate crop extraction using multi-source remote sensing images. The main objective of this study is to integrate Sentinel-1 and Sentinel-2 satellite images for the Rahim Yar Khan district and to compare the classification performance of the Random Forest algorithm using Sentinel-1 (VV, HV, and VV+HV), Sentinel-2, and integrated datasets.

Material and Methods:

Description of the Study Area:

The Rahim Yar Khan district is located between 60°44' and 70°02' East and 27°41' and 29°15' North (Figure 1). Covering an area of 11,880 km², the district experiences extremely hot and dry summers, with temperatures ranging from 6.8°C to 49.7°C and an average annual rainfall of 165 mm. The district is divided into three main regions: the river region, the irrigated region, and the Cholistan region. The irrigated area, situated to the southwest of the river region, is adjacent to the Indus and Panjnad rivers and has elevations between 150 and 200 meters above sea level. The Cholistan Desert, located in the southeast, is characterized by its arid conditions. Major crops in the district include sugarcane, wheat, and cotton. The principal industries are textile spinning, vegetable ghee production, and sugar, along with oil mills, paper production, and pharmaceuticals.

In this study, Sentinel-1 and Sentinel-2 data were used, along with ground truth information, to classify crops using a Random Forest classifier (Figure 2).

Satellite Data Used:

This study utilized the ground range detected (GRD) product from Sentinel-1A in Interferometric Wide (IW) mode, which provides a fine spatial resolution of 10 meters. This data source includes two primary polarization channels: VV (vertical-vertical) and VH (vertical-horizontal), available in Google Earth Engine (GEE) [12]. The images were acquired throughout

the kharif crop growing season, from May to October 2022, to cover the entire crop cycle from planting to harvesting for mapping purposes. Additionally, multispectral optical imagery from Sentinel-2 was used. Sentinel-2 imagery includes 13 spectral bands across the visible, near-infrared (NIR), and shortwave infrared (SWIR) regions of the electromagnetic spectrum (Table 1), with spatial resolutions ranging from 10 to 60 meters. Sentinel-2 provides frequent revisits, with a 10-day interval for a single satellite and a 5-day interval when both satellites are operational [2]. For this study, Sentinel-2 optical images of Rahim Yar Khan with minimal cloud cover (less than 10%) acquired between early May and October 2022 were used. Cloudy pixels were masked using the Quality Assessment band, and a median reduction was applied to produce a seasonal composite image for time series analysis. Vegetation indices commonly used in the analysis include the Normalized Difference Vegetation Index (NDVI) [16], Soil-Adjusted Vegetation Index (SAVI) [17], Bare Soil Index (BSI) [18], and Enhanced Vegetation Index (EVI) [16].

$$\mathrm{NDVI} = \frac{\mathrm{NIR}_\sigma - \mathrm{Red}_\sigma}{\mathrm{NIR}_\sigma + \mathrm{Red}_\sigma} \quad (1)$$

$$\mathrm{SAVI} = \frac{(\mathrm{NIR}_\sigma - \mathrm{REd}_\sigma)}{(\mathrm{NIR}_\sigma - \mathrm{Red}_\sigma + \mathrm{L})} \times (1 + \mathrm{L}) \quad (2)$$

$$\mathrm{BSI} = \left(\frac{(\mathrm{PRED}_\sigma + \mathrm{PSWIR1}_\sigma) - (\mathrm{PNIR}_\sigma + \mathrm{PBLUE}_\sigma)}{(\mathrm{PRED}_\sigma + \mathrm{PSWIR1}_\sigma) + (\mathrm{PNIR}_\sigma + \mathrm{PBLUE}_\sigma)}\right) + 1 \quad (3)$$

$$\mathrm{EVI} = 2.5 = \left(\frac{\mathrm{NIR}_\sigma - \mathrm{REd}_\sigma}{(\mathrm{NIR}_\sigma + 6\mathrm{red} - 7.5\ \mathrm{Blue}) + 1}\right) \quad (4)$$

Where $\mathrm{PBLUE}_\sigma, \mathrm{NIR}_\sigma$ and Red_σ represents reflectance in the blue, NIR and red wavebands, respectively.

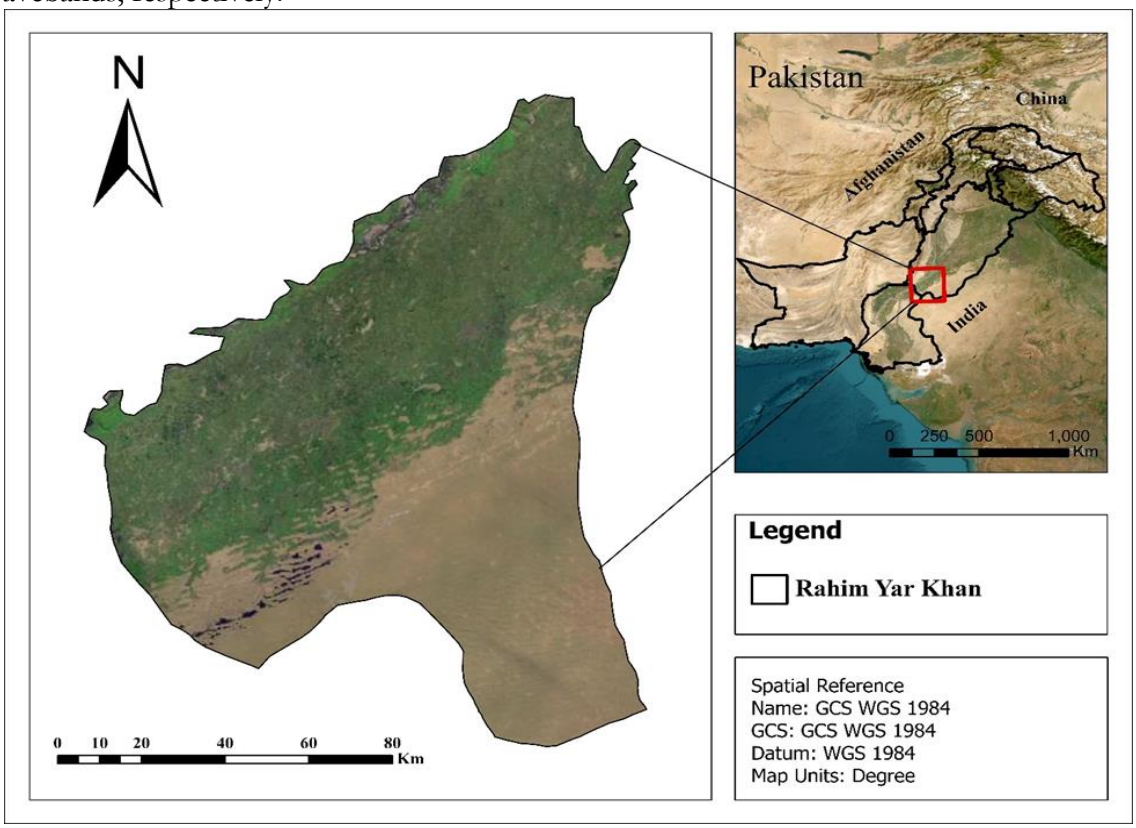


Figure 1: The Study area map of District Rahim Yar Khan

Ground Truth Information and Sample Data:

While crops were the primary focus, the study also addressed regional heterogeneity and other misclassifications by defining broad LCLU (Land Cover/Land Use) groups. These categories included Barren, Built-up, Water Bodies, Cotton, Orchard, Rice, Sugarcane, and Other Crops (Table 2, Figure 3). To evaluate the performance of supervised classification for

crop mapping, reference samples from the 2022 growing season (May to September) were collected. These data enabled the assessment, modeling, and quantification of agricultural crop productivity. For Rahim Yar Khan, the reference samples were divided into training and validation sets (70% and 30%, respectively) to train and evaluate the supervised classification system. Although the study primarily focused on agricultural crops, the spatial variability of the region meant that other land cover classes could influence crop mapping outcomes. The study area's grassland consisted of various small plants, while built-up areas included dwellings and impermeable surfaces. Barren land covered all uncultivated areas, and water bodies included lakes, rivers, streams, and other still water sources. The 'Other' category encompassed any class not explicitly included in the predefined categories. The classes were determined through on-screen analysis of multi-sensor composites and Google Earth geo-referenced images. In addition to the sugarcane, cotton, rice, and orchard samples, additional training and validation points were randomly selected. On-screen digitizing was performed to create polygons encompassing each sampling point. Seven major land use and land cover groups were identified within the area of interest, corresponding to the target crops.

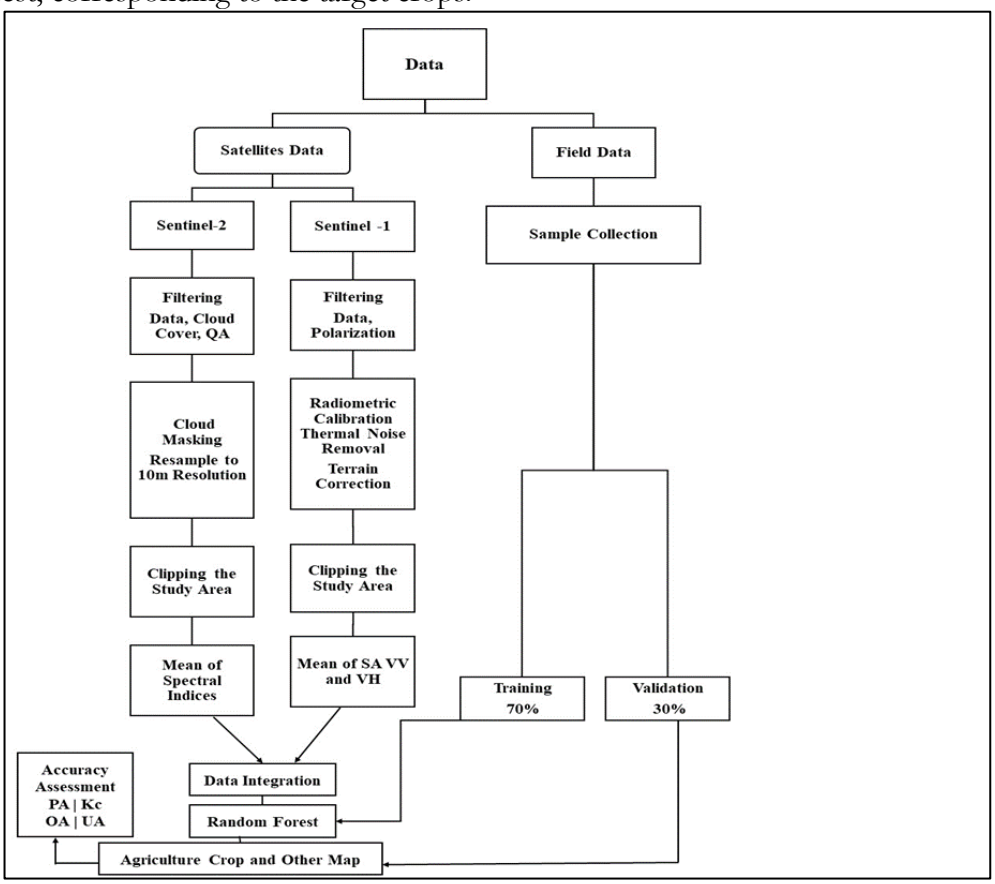


Figure 2: Flowchart of Crop Classification Using Random Forest Algorithm

Table 1: Characteristics of both Sentinel 1 and Sentinel 2 Sensors used in this Study.

Satellite	Band No	Wavelength(nm)	Band Name	Resolution (m)
Sentinel-1		C-band	VV	10
			VH	10
	2	490	Blue	10
	3	560	Green	10
	4	665	Red	10
Sentinel-2	8	842	Near-infrared	10
	11	1610.4	SWIR	20
	12	2202.4	SWIR	20

Table 2: Distribution of training and validation samples for LCLU classification in the study area

No	LCLU Class	Count	Training Sample	Validation Sample
1	Barren	102	71	31
2	Built up	119	83	36
3	Cotton	100	70	30
4	Orchard	100	70	30
5	Other Crop	108	75	33
6	Rice	100	70	30
7	Sugarcane	242	170	72
8	Water-bodies	101	70	31

Table 2 shows that approximately 70% of the field samples were used to train classification models, such as Random Forest, selected for their capability to perform multi-class classification tasks and manage non-linear data relationships. The remaining 30% of the field samples were reserved for model validation. This data was used to create agricultural crop and other land cover maps, serving as ground truth standards for evaluating model accuracy.

Random Forest Algorithm:

Random Forest (RF) is an ensemble classifier that uses multiple decision trees to overcome the limitations of individual trees [19]. In this study, the `tune` function was employed to select random parameters. The optimal number of predictors/features (`max features`) was calculated as the square root of the total available features, and the ideal number of trees (`mtry`) was set to 100. One of the advantages of RF is its ability to identify significant information within each feature. By incorporating numerous trees, RF addresses the issues that may arise from relying on a single tree, helping to reach a global optimum. This classifier effectively handles large datasets and uneven input features, producing highly accurate results [20]. Typically, the sample data are divided into two parts: training datasets for model construction and test datasets for model validation [12]. RF has been widely used in agriculture, though one of its drawbacks is the difficulty in visualizing the numerous trees involved [21]. In this study, the RF classifier in Google Earth Engine (GEE) was utilized to obtain LCLU classification from Sentinel-1 (VV), Sentinel-1 (VH), Sentinel-1 (VV+VH), Sentinel-2 optical multispectral bands, and integrated datasets from Sentinel-1 and Sentinel-2.

Accuracy Assessment:

Accuracy assessment of the LCLU is a crucial component of the classification process [22]. It is commonly measured by the degree of agreement between the classification results and the presumed true values [23]. The classification outcomes were evaluated using confusion matrices to calculate overall accuracy (OA) (Eq 5), producer accuracy (PA), user accuracy (UA), the kappa coefficient (Eq 6), and the F1-score (Eq 7) [22]. Overall accuracy reflects the proportion of correctly classified reference pixels relative to the total number of reference pixels.

$$\left(\mathrm{OA} = \frac{\sum \text{correct predictions}}{\text{total number of predictions}}\right) \quad (5)$$

In Equation 6, predictions were made for all available validation samples, and the predicted labels were then compared to the true labels [8].

$$\text{Kappa Coefficient (KC)} = \mathrm{N}\sum \mathrm{ri} = 1xii - \sum \mathrm{ri} = 1(xi + x + \mathrm{i})\mathrm{N}2 - \sum \mathrm{ri} = (xi + x + \mathrm{i}) \quad (6)$$

Classified maps were evaluated using the F1-Score method, Eq (7), which calculates accuracy assessment statistics for each class based on confusion matrices. The F1 score, which is the harmonic mean of recall and precision, serves as a crucial metric for assessing both user accuracy and producer accuracy [24]. This metric provides a more comprehensive evaluation of the classification model's performance compared to independent producer and user accuracy indicators.

$$F1 = \frac{2 \times PA \times UA}{PA + UA} \quad (7)$$

Where PA represents producer accuracy, and UA represents user accuracy.

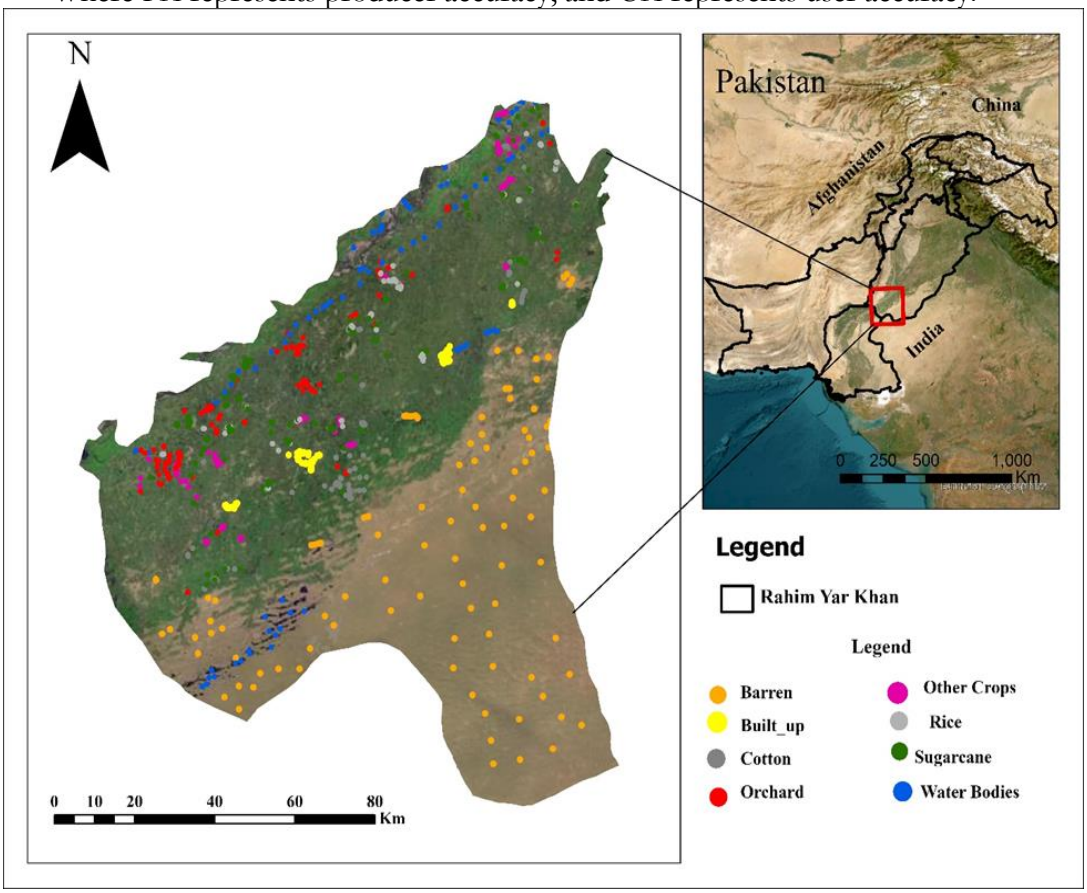


Figure 3: Sample Area of Rahim Yar Khan District

Result and Discussion:

Agricultural crops in the Rahim Yar Khan district were mapped at a 10-meter resolution by integrating Sentinel-2 and Sentinel-1 satellite data using the Random Forest (RF) machine learning method on the Google Earth Engine (GEE) cloud computing platform. Multispectral data from Sentinel-2, along with VV and VH cross-polarizations from Sentinel-1, were utilized for crop classification. The resulting maps accurately depict cropland and various land cover types, demonstrating the effectiveness of this approach in categorizing crops such as sugarcane, cotton, rice, orchards, water bodies, deserts, and built-up areas. Various combinations of optical data from Sentinel-2 and microwave data from Sentinel-1 were tested using RF for crop classification (Table 3). These combinations included optical bands from Sentinel-2, the VH polarization band from Sentinel-1, the VV polarization band from Sentinel-1, a combination of VH and VV polarization bands from Sentinel-1, and a combination of optical bands from Sentinel-2 with both VH and VV polarization bands from Sentinel-1. Area statistics for different crops from the Crop Reporting Service (CRS) for 2022 were used as a reference for comparison with the satellite-based crop predictions.

Table 3: Area of different crops (in km^2) predicted by using different combination of Sentinel-1 and Sentinel-2 imagery and crop area from crop reporting service for the year 2022.

Class Name	Sentinel-2	Sentinel-1 VH	Sentinel-1 VV	Sentinel-1 VH+VV	Combined Multi-sensor Year 2022	CRS 2022
Sugarcane	1762.7	2581.4	3290.3	2707.1	1834.7	2165.0
Cotton	1717.6	1355.6	836.3	1474.2	1578.6	1897.9
Rice	212.3	989.4	835.7	781.6	204.4	283.2

Other Crop	2450.2	1695.9	1588.5	1704.9	2891.5	834.2
Orchard	58.5	199.4	213.9	137.1	54.31	196
Water Bodies	502.2	587.1	388.7	360.3	305.4	-
Desert	5386.6	4942.8	5088.2	5231.3	5524.0	-
Built up	504.3	234.0	343.9	189.1	192.8	-

Table 3 shows that the combination of Sentinel-1 and Sentinel-2 data estimates the sugarcane area as 1834.71 km², which is relatively close to the 2165.07 km² estimate provided by the Crop Reporting Service (CRS). In contrast, for other band combinations, there is a significant discrepancy between the satellite-based crop area estimates and those from CRS. Similarly, for cotton and rice, the satellite-based crop area estimates using the Sentinel-1 and Sentinel-2 combination are also close to the CRS estimates, as shown in Table 3.

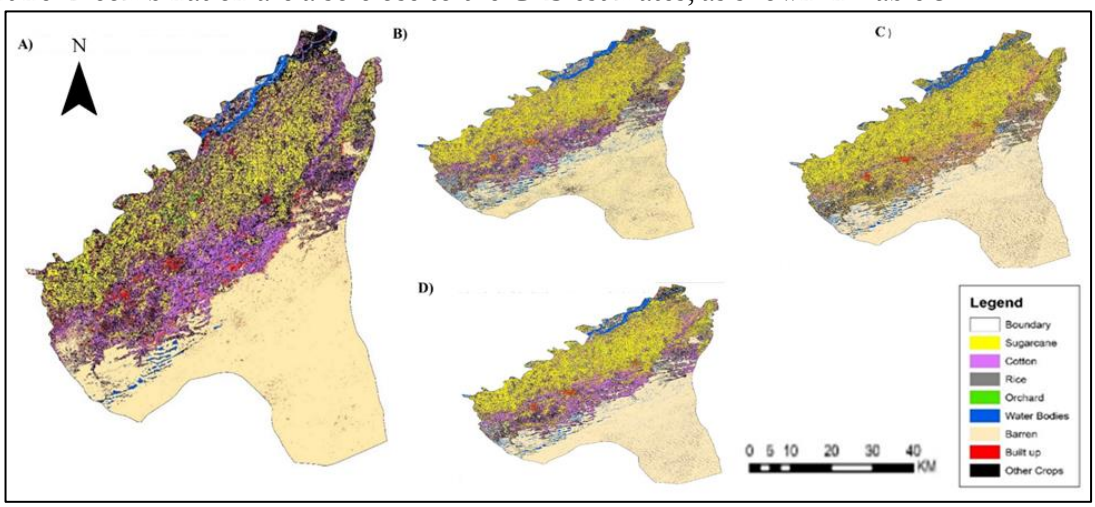


Figure 4: Classified maps of Rahim Yar Khan District using Sentinel-1 and Sentinel-2 (A)Crop Classification using Sentinel 2 Sensor Only (B) Crop Classification using Sentinel 1 VH Channel (C) Crop Classification using Sentinel 1 VV Channel (D) Crop Classification using Sentinel-1 VH +VV Channel.

To evaluate the accuracy of different combinations of Sentinel-1 and Sentinel-2 data for crop classification using the Random Forest (RF) method, various accuracy metrics were employed, including overall accuracy (OA), F1-score, Kappa coefficient (KC), user accuracy (UA), and producer accuracy (PA). These metrics were assessed for key crops (sugarcane, rice, cotton, orchards) and other land cover types in the Rahim Yar Khan District. Our results demonstrate high values for F1-score, user accuracy, and producer accuracy for the combination of Sentinel-1 and Sentinel-2 data compared to the other four combinations (Table 4).

The integration of Sentinel-2 and Sentinel-1 data, applied at a 10-meter resolution using the RF machine learning approach on the Google Earth Engine (GEE) platform, yielded promising results. This approach produced accurate maps that effectively depicted crops and various land cover types by combining multispectral data from Sentinel-2 with VV and VH cross-polarization bands from Sentinel-1. The method successfully classified multiple land cover types, including water bodies, deserts, and built-up areas, as well as crops like rice, cotton, sugarcane, and orchards. This highlights the approach's effectiveness in distinguishing and categorizing agricultural areas.

A comparative study using Crop Reporting Service (CRS) data for 2022 confirmed the accuracy of the satellite-based forecasts. For rice, cotton, and sugarcane, the crop area estimates from combining Sentinel-1 and Sentinel-2 data closely matched the CRS data. For instance, the estimated sugarcane area was 1834.71 km², which aligns well with the 2165.07 km² estimate from CRS. In contrast, other satellite data combinations showed significant discrepancies, underscoring the superiority of the integrated approach for accurate crop area calculations.

Table 4: Accuracy of Random Forest Algorithm Using Different Datasets on District Rahim Yar Khan

RF 2022 over		Sugarcane	Cotton	Rice	Other crops	Orchard	Water Bodies	Barren	Built up	OA	KC
RF VH	PA (%)	0.85	0.91	0.53	0.51	0.25	0.64	0.83	0.63	0.66	0.60
	UA (%)	0.54	0.78	0.78	0.75	0.42	0.78	0.71	0.82		
	F Score	0.66	0.84	0.63	0.61	0.31	0.70	0.76	0.71		
RF VV	PA (%)	0.82	0.5	0.39	0.27	0.25	0.75	0.83	0.86	0.62	0.58
	UA (%)	0.45	0.63	0.61	0.36	0.72	0.80	0.80	1.0		
	F Score	0.58	0.55	0.47	0.31	0.37	0.77	0.81	0.92		
RF VH+VV	PA (%)	0.91	0.91	0.53	0.48	0.25	0.67	0.93	0.88	0.72	0.67
	UA (%)	0.56	0.78	0.93	0.7	0.61	0.90	0.77	0.94		
	F Score	0.69	0.84	0.68	0.57	0.35	0.77	0.84	0.91		
RF 2022 over Sentinel-2	PA (%)	0.98	0.95	0.82	0.86	0.59	0.96	0.93	0.97		
	UA (%)	0.77	0.88	1.0	0.89	0.95	1.0	0.96	0.94	0.89	0.87
	F Score	0.86	0.91	0.90	0.87	0.73	0.98	0.94	0.95		
RF 2022 Combined Multi-Sensor	PA (%)	1.0	1.0	0.78	0.87	0.62	1.0	1.0	0.86		
	UA (%)	0.96	0.88	1.0	0.96	1.0	1.0	1.0	1.0	0.93	0.90
	F Score	0.87	0.94	0.88	0.90	0.76	1.0	1.0	1.0		

The combined Sentinel-1 and Sentinel-2 approach consistently achieved high values across all accuracy evaluation metrics used in the study: overall accuracy (OA), F1-score, Kappa coefficient (KC), user accuracy (UA), and producer accuracy (PA). These results highlight the

potential of merging advanced machine learning algorithms with optical and microwave satellite data to enhance land cover categorization and agricultural monitoring. This integrated approach offers a reliable tool for resource management and planning in agricultural regions.

The study's findings, which include timely and precise crop classification maps, significantly enhance agricultural management. By using these maps, farmers can better plan their planting, irrigation, and harvesting operations, thereby increasing yields and improving resource efficiency. For food security initiatives, the study provides a scalable and cost-effective method for monitoring and estimating crop output. Early identification of regions at risk for low yields or crop failure allows for prompt intervention, while accurate crop mapping supports resilient agricultural practices and policies, contributing to long-term food security by tracking agricultural trends and assessing the impact of climate change.

Conclusion:

The use of remote sensing (RS) has rapidly expanded in recent years, thanks to the availability of high spatial resolution Sentinel-2 and Sentinel-1 data, offered free of charge, and the high-performance cloud computing platforms like Google Earth Engine (GEE) for processing and analyzing large datasets. This study demonstrates that integrating the state-of-the-art Random Forest (RF) machine learning method with Sentinel-2 and Sentinel-1 data results in a crop classification map with higher accuracy compared to traditional statistical classification methods and single-satellite data. The primary objective of the research was to map and classify crop cover in Rahim Yar Khan District, Pakistan. Various combinations of satellite data were tested, including optical bands from Sentinel-2, VH polarization from Sentinel-1, VV polarization from Sentinel-1, a combination of VH and VV polarization bands from Sentinel-1, and a combination of optical bands from Sentinel-2 with VH and VV polarization bands from Sentinel-1. Our results indicate that the combination of Sentinel-1 and Sentinel-2 outperforms the use of individual optical or SAR imagery. For future research, incorporating very high-resolution imagery from sources such as WorldView, GeoEye, and Pleiades, along with advanced machine learning methods like Support Vector Machine (SVM) and Artificial Neural Networks (ANN), could further enhance the accuracy of crop classification.

Acknowledgement:

I would like to express my sincere gratitude to the Crop Reporting Services for their essential contribution to this study. I am also grateful for the cooperation of the Urban Unit, which was instrumental to the success of this research. Additionally, I extend my appreciation to the European Space Agency for providing access to Sentinel-1 and Sentinel-2 satellite imagery, which was crucial for the analysis and classification of crops.

Author's Contribution:

All the authors had different contributions to this research work and are mentioned here accordingly. Conceptualization (S.A, M.U), formal analysis (F.U, A.A), methodology (M.U, F.U, A.A and S.A), writing—original draft preparation (F.U, Z.A.A, A.A, S.A), writing—review and editing (S.A, A.A, Z.A.A, M.U, S.M.I), visualization (S.U.K and S.M.I) All authors have read and agreed to the published version of the manuscript.

Conflict of Interest: The authors declare they have no conflict of interest in publishing this manuscript in this Journal.

References:

[1] Asia and the Pacific Regional Overview of Food Security and Nutrition 2022. FAO, 2023. doi: 10.4060/cc3990en.

[2] G. A. Abubakar et al., "Mapping Maize Cropland and Land Cover in Semi-Arid Region in Northern Nigeria Using Machine Learning and Google Earth Engine," Remote Sens., vol. 15, no. 11, p. 2835, May 2023, doi: 10.3390/rs15112835.

[3] M. Majeed et al., "Prediction of flash flood susceptibility using integrating analytic hierarchy process (AHP) and frequency ratio (FR) algorithms," Front. Environ. Sci., vol.

10, no. January, pp. 1–14, 2023, doi: 10.3389/fenvs.2022.1037547.

[4] J. Wang et al., "Mapping sugarcane plantation dynamics in Guangxi, China, by time series Sentinel-1, Sentinel-2 and Landsat images," Remote Sens. Environ., vol. 247, p. 111951, Sep. 2020, doi: 10.1016/j.rse.2020.111951.

[5] V. Tiwari et al., "Wheat Area Mapping in Afghanistan Based on Optical and SAR Time-Series Images in Google Earth Engine Cloud Environment," Front. Environ. Sci., vol. 8, Jun. 2020, doi: 10.3389/fenvs.2020.00077.

[6] Y. Durgun, A. Gobin, R. Van De Kerchove, and B. Tychon, "Crop Area Mapping Using 100-m Proba-V Time Series," Remote Sens., vol. 8, no. 7, p. 585, Jul. 2016, doi: 10.3390/rs8070585.

[7] A. Elders et al., "Estimating crop type and yield of small holder fields in Burkina Faso using multi-day Sentinel-2," Remote Sens. Appl. Soc. Environ., vol. 27, p. 100820, Aug. 2022, doi: 10.1016/j.rsase.2022.100820.

[8] K. Van Tricht, A. Gobin, S. Gilliams, and I. Piccard, "Synergistic Use of Radar Sentinel-1 and Optical Sentinel-2 Imagery for Crop Mapping: A Case Study for Belgium," Remote Sens., vol. 10, no. 10, p. 1642, Oct. 2018, doi: 10.3390/rs10101642.

[9] Y. Pageot, F. Baup, J. Inglada, N. Baghdadi, and V. Demarez, "Detection of Irrigated and Rainfed Crops in Temperate Areas Using Sentinel-1 and Sentinel-2 Time Series," Remote Sens., vol. 12, no. 18, p. 3044, Sep. 2020, doi: 10.3390/rs12183044.

[10] G. R. Aduvukha et al., "Cropping Pattern Mapping in an Agro-Natural Heterogeneous Landscape Using Sentinel-2 and Sentinel-1 Satellite Datasets," Agriculture, vol. 11, no. 6, p. 530, Jun. 2021, doi: 10.3390/agriculture11060530.

[11] S. Felegari et al., "Integration of Sentinel 1 and Sentinel 2 Satellite Images for Crop Mapping," Appl. Sci., vol. 11, no. 21, p. 10104, Oct. 2021, doi: 10.3390/app112110104.

[12] C. Li et al., "Mapping Winter Wheat with Optical and SAR Images Based on Google Earth Engine in Henan Province, China," Remote Sens., vol. 14, no. 2, Jan. 2022, doi: 10.3390/rs14020284.

[13] S. Asam, U. Gessner, R. Almengor González, M. Wenzl, J. Kriese, and C. Kuenzer, "Mapping Crop Types of Germany by Combining Temporal Statistical Metrics of Sentinel-1 and Sentinel-2 Time Series with LPIS Data," Remote Sens., vol. 14, no. 13, p. 2981, Jun. 2022, doi: 10.3390/rs14132981.

[14] N. Gorelick, M. Hancher, M. Dixon, S. Ilyushchenko, D. Thau, and R. Moore, "Google Earth Engine: Planetary-scale geospatial analysis for everyone," Remote Sens. Environ., vol. 202, pp. 18–27, Dec. 2017, doi: 10.1016/j.rse.2017.06.031.

[15] W. Zhang, M. Brandt, A. V. Prishchepov, Z. Li, C. Lyu, and R. Fensholt, "Mapping the Dynamics of Winter Wheat in the North China Plain from Dense Landsat Time Series (1999 to 2019)," Remote Sens., vol. 13, no. 6, p. 1170, Mar. 2021, doi: 10.3390/rs13061170.

[16] A. Huete, K. Didan, T. Miura, E. . Rodriguez, X. Gao, and L. . Ferreira, "(NDVI EVI)Overview of the radiometric and biophysical performance of the MODIS vegetation indices," Remote Sens. Environ., vol. 83, no. 1–2, pp. 195–213, Nov. 2002, doi: 10.1016/S0034-4257(02)00096-2.

[17] A. . Huete, "A soil-adjusted vegetation index (SAVI)," Remote Sens. Environ., vol. 25, no. 3, pp. 295–309, Aug. 1988, doi: 10.1016/0034-4257(88)90106-X.

[18] N. Mzid, S. Pignatti, W. Huang, and R. Casa, "An Analysis of Bare Soil Occurrence in Arable Croplands for Remote Sensing Topsoil Applications," Remote Sens., vol. 13, no. 3, p. 474, Jan. 2021, doi: 10.3390/rs13030474.

[19] Y. He, E. Lee, and T. A. Warner, "A time series of annual land use and land cover maps of China from 1982 to 2013 generated using AVHRR GIMMS NDVI3g data," Remote Sens. Environ., vol. 199, pp. 201–217, Sep. 2017, doi: 10.1016/j.rse.2017.07.010.

[20] V. F. Rodriguez-Galiano, B. Ghimire, J. Rogan, M. Chica-Olmo, and J. P. Rigol-Sanchez, "An assessment of the effectiveness of a random forest classifier for land-cover classification," ISPRS J. Photogramm. Remote Sens., vol. 67, pp. 93–104, Jan. 2012, doi: 10.1016/j.isprsjprs.2011.11.002.

[21] L. Breiman, "machine Learning," Mach. Learn., vol. 45, no. 1, pp. 5–32, 2001, doi: 10.1023/A:1010933404324.

[22] A. F. Koko, Y. Wu, G. A. Abubakar, A. A. N. Alabsi, R. Hamed, and M. Bello, "Thirty Years of Land Use/Land Cover Changes and Their Impact on Urban Climate: A Study of Kano Metropolis, Nigeria," Land, vol. 10, no. 11, p. 1106, Oct. 2021, doi: 10.3390/land10111106.

[23] A. Tassi and M. Vizzari, "Object-Oriented LULC Classification in Google Earth Engine Combining SNIC, GLCM, and Machine Learning Algorithms," Remote Sens., vol. 12, no. 22, p. 3776, Nov. 2020, doi: 10.3390/rs12223776.

[24] D. Chicco and G. Jurman, "The advantages of the Matthews correlation coefficient (MCC) over F1 score and accuracy in binary classification evaluation," BMC Genomics, vol. 21, no. 1, p. 6, Dec. 2020, doi: 10.1186/s12864-019-6413-7.

Copyright © by authors and 50Sea. This work is licensed under Creative Commons Attribution 4.0 International License.